Accepted Manuscript

A benzothiazole-rhodol based luminophor: ESIPT-induced AIE and an application for detecting Fe2+ ion

Jianping Guan, Qin Tu, Long Chen, Mao-Sen Yuan, Jinyi Wang

PII: S1386-1425(19)30495-0
DOI: https://doi.org/10.1016/j.saa.2019.05.019
Reference: SAA 17114
To appear in: *Spectrochimica Acta Part A: Molecular and Biomolecular Spectroscopy*
Received date: 14 March 2019
Revised date: 10 May 2019
Accepted date: 10 May 2019

Please cite this article as: J. Guan, Q. Tu, L. Chen, et al., A benzothiazole-rhodol based luminophor: ESIPT-induced AIE and an application for detecting Fe2+ ion, Spectrochimica Acta Part A: Molecular and Biomolecular Spectroscopy, https://doi.org/10.1016/j.saa.2019.05.019

A Benzothiazole-rhodol Based Luminophor: ESIPT-induced AIE and an Application for Detecting Fe^{2+} Ion

Jianping Guan [1#], Qin Tu [1#], Long Chen[1], Mao-Sen Yuan [1,2*] & Jinyi Wang[1]

[1]*College of Chemistry & Pharmacy, Northwest A&F University, Yangling, Shaanxi 712100, P. R. China*

[2] *State Key Laboratory of Crystal Materials, Shandong University, Jinan, 250100, China*

 # Authors contributed equally

** Corresponding author. Tel/fax: +86-29-87082520.*

E-mail address: yuanms@nwsuaf.edu.cn (M.-S. Yuan).

Abstract

Herein, we designed and synthesized a luminophor, **Rh-F**, which is an intergrant of rhodol and 2-hydroxy benzothiazole by introducing a benzothiazole unit onto the ortho-position of the phenolic hydroxy of rhodol. **Rh-F** exhibited excellent fluorescence properties such as a large Stokes shift (>180 nm) and the synergistic effect of aggregation-induced emission (AIE) and an excited state intramolecular proton transfer (ESIPT) feature. The AIE/ESIPT mechanism was thoroughly explored using X-ray single-crystal structures and photophysical determinations. Furthermore, **Rh-F** showed a sensitive fluorescence response to Fe^{2+} with low detection limits of 115.2 nM and high selectivity. Studies of its sensing mechanism indicated that the Fe^{2+}-induced blue-green fluorescence-quenched at 525 nm originates from an irreversible Fe^{2+} chelate with the oxygen atom of the hydroxyl group and the N atom of the benzothiazole moiety. This blocked the ESIPT process of **Rh-F** which resulted in the quenching of the fluorescence sensor for **Rh-F**.

Keywords: Luminophor, ESIPT, AIE, Detect, Fe^{2+}

1. Introduction

In recent years, an increasing number of new fluorophores based on aggregation-induced emission (AIE) or excited state intramolecular proton transfer (ESIPT) mechanisms have been used in organic optoelectronic materials [1-3], molecular probes [4-6], and in various laser dyes [7-9]. As we know, ESIPT is a photo-induced proton transfer through an intramolecular hydrogen bond. Its large Stokes shift is beneficial for the prevention self-absorption of fluorophores and increases efficiency [10-11]. ESIPT-based illuminants display excellent signal performance on account of dual emission in aqueous solution: enol-form emission and keto-form emission [9,12]. This possess excellent photostability and spectral sensitivity to the surrounding medium [13]. In addition, an AIE phenomenon was reported by Tang et al. in 2001 which is completely opposite to the aggregation-caused quenching (ACQ) effect [14]. At present, most of the reported AIE molecules show high solid-state luminous efficiency, high concentration of aggregation-induced emission, and background signals that are easy to eliminate [15], so they have been widely used in the development of organic optoelectronic materials and fluorescent biosensors.

To combine AIE and ESIPT is an effective strategy to improve the photophysical properties of the illuminants. The unique advantages of AIE/ESIPT dual-mechanism fluorophores result from the following two aspects. On the one hand, the AIE characteristics of the fluorophore facilitate the induction of the ESIPT process with large Stokes shift emission by forming aggregates, especially in very polar or strong hydrogen bonding solvents. On the other hand, the ESIPT process can also enhance the AIE effect by intramolecular hydrogen bonding, resulting in enhanced fluorescence in the aggregated state [16]. These advantages are not available with a single AIE or ESIPT fluorophore.

Therefore, this kind of novel double-system (AIE/ESIPT) fluorophore with a large Stokes shift, strong light stability, and no self-quenching at high concentrations has great potential for application in the development of bioimaging sensors and organic photoelectric materials.

Iron is one of the essential trace elements of biological systems and it is an indispensable substance in many physiological processes. Iron is generally present in the form of ferrous and trivalent iron. Creatures mainly use ferrous iron because ferrous iron is easier to be assimilated than trivalent iron. Iron deficiency or poor iron use will result in anemia, fatigue, decreased immunity and it will eventually cause a variety of diseases. If iron ion concentration surpasses the normal level, it may lead to liver and kidney damage, cardiovascular disease, and heart disorders. At the same time, iron ion is also a major environmental pollutant. Based on the importance of iron ions in the function of organisms and in the environment, it is of great significance to detect iron ions in clinical, medical, health, environmental, and other aspects [17-20]. So far, many fluorescent probes have been developed to detect iron ions, such as Schiff base, crown ether, imidazole, leptin, fluorescein, naphthalimide, rhodamine, and so on [21-29]. However, most of these fluorescent sensors are applied for the detection of Fe^{3+}. There has been little research for detecting Fe^{2+} and many methods lack selectivity and sensitivity. Therefore, it is still a great challenge to develop highly selective, sensitive, and efficient chemosensors for detection of Fe^{2+}.

Rhodol (or rhodafluor), which can be regarded as a mixture of rhodamine and fluorescein, exhibits many excellent photophysical properties (i.e., high photostability, high fluorescence quantum yield, and good solubility) [30-33]. In this study, we designed and synthesized a new benzothiazole-modified rhodol luminophore, **Rh-F**, by introducing a benzothiazole unit onto the ortho-position of the phenolic hydroxyl of rhodol dyes (Scheme 1). **Rh-F** possess excellent AIE and ESIPT

fluorescence properties. Furthermore, in this molecular structure, the formative 2-hydroxy benzothiazole can be used as the sensor site to recognize Fe^{2+} through blocking ESIPT responding mechanisms. We deeply explored the new AIE/ESIPT-active luminophor and clarified the AIE/ESIPT mechanism. As a fluorescent chemodosimeter, **Rh-F** was successfully demonstrated to be useful for the discriminative detection of Fe^{2+} in aqueous solution. A significant decrease in the blue-green fluorescence at 525 nm and a color change from colorless to yellow induced by Fe^{2+} was observed.

2. Experimental Section

2.1. Materials

All chemicals in this study were purchased from Energy chemical or Aladdin Reagent Company and used without any further purification. The liquid solvents used for the synthesis and analysis were analytical grade. Column chromatography purification generally used silica gel (200-300 mesh) for the separations. The metal salt solutions were all formulated using Milli-Q system purified water (purified to 18.2 MΩ).

2.2. Instruments and methods

^{1}H-nuclear magnetic resonance (NMR) and ^{13}C NMR spectra of the products were recorded on a Bruker 500 MHz/125 MHz NMR spectrometer using tetramethylsilane (TMS) as the internal standard (chemical shifts in ppm). High-resolution mass spectral data of the product were obtained using a Thermo LTQ-Orbitrap mass spectrometer. UV–vis absorption spectra were measured by using a Shimadzu UV1780 spectrometer (Shimadzu, Japan), and fluorescence emission spectra measurements were performed on a Shimadzu RF-5301 fluorescence spectrometer (Shimadzu,

Japan). The single crystal of compound **Rh-F** was obtained by the slow diffusion of THF/cyclohexane solutions over several days at room temperature. The data collection was done at room temperature on a Bruker SMART APEX-II CCD area detector using graphite-mono-chromated Mo Ka radiation (λ=0.71073 Å). Data reduction and integration together with global unit cell refinements were done by the INTEGRATE program of the APEX2 software. Semi-empirical absorption corrections were applied using the SCALE program for the area detector. The structure was solved by direct methods and refined by full matrix least-squares methods on F2 using SHELX.

2.3. Synthetic procedures

*2.3.1 Synthesis of compound **4**.*

To a suspended solution of **3** (0.52 g, 1 mmol) in ethanol (20 mL) was added an excess of Ethylenediamine (3.2 mL, 90%) and the reaction mixture was refluxed under nitrogen for 24 h with stirring. The reaction mixture was cooled to room temperature and concentrated under vacuum. The resulting residue was finally purified by silica gel chromatography (CH_2Cl_2: CH_3OH = 30:1, *v/v*) to afford compound **4** as a pale white solid (0.31 g, 67.6% yield).: mp 247 – 248 °C. ^{1}H NMR (500 MHz, $CDCl_3$): δ_H (500 MHz, $CDCl_3$) 12.79 (1 H, s), 8.64 (1 H, s), 8.06 (1 H, d, *J* 5.0), 7.97 (1 H, d, *J* 7.9), 7.83 (1 H, d, *J* 7.9), 7.59 (2 H, d, *J* 4.1), 7.51 (1 H, t, *J* 7.4), 7.41 (1 H, t, *J* 7.4), 8.90 – 6.06 (15 H, m), 7.31 (1 H, s), 7.17 (1 H, d, *J* 5.2), 6.98 (2 H, d, *J* 19.6), 6.50 (2 H, d, *J* 11.7), 6.38 (1 H, d, *J* 8.8), 3.41 (5 H, d, *J* 7.1), 3.67 – 2.82 (8 H, m), 3.19 (2 H, dd, *J* 37.3, 8.9), 1.66 (2 H, s), 1.73 – 1.14 (7 H, m), 1.30 (1 H, s), 1.24 (6 H, t, *J* 6.6); ^{13}C NMR (125 MHz, $CDCl_3$): *δ* 169.81, 167.92, 159.32 155.16, 152.68, 151.35, 149.43, 133.58, 132.26, 129.06, 128.03, 127.97, 126.81, 125.70, 123.95, 123.41, 122.08, 121.54, 114.62 111.24 109.37, 104.89 97.99 77.32, 77.07, 76.81, 67.12, 49.18, 44.51, 40.23, 29.73,12.55; HRMS (ESI, *m/z*): Calcd. for $[C_{33}H_{30}N_4O_3S - H]^-$, 563.22; Found, 563.209.

*2.3.2 Synthesis of compound **Rh-F***

To a suspended solution of **4** (54 mg, 0.1 mmol) in 1,4-dioxane (3 mL) was added an excess of Sodium borohydride (25 mg, 0.6 mmol) and Trifluoroacetic acid (800 μL). Next , the solution was heated at 80 °C under nitrogen for 8 h with stirring. The reaction mixture was cooled to room temperature and concentrated under vacuum. The resulting residue was finally purified by silica gel chromatography (CH_2Cl_2: CH_3OH = 80:1, *v/v*) to afford compound **Rh-F** as a pale white solid (28.2 mg, 42.8% yield). mp 195 – 196 °C. ^{1}H NMR (500 MHz, $CDCl_3$): δ 12.85 (s, 1H), 8.61 (1 H, s), 8.02 (2 H, dd, *J* 47.1, 6.1), 7.82 (1 H, d, *J* 7.3), 7.62 – 7.44 (3 H, m), 7.41 (1 H, d, *J* 7.0), 9.01 – 6.21 (14 H, m), 7.31 (1 H, s), 7.17 (1 H, d, *J* 5.1), 6.98 (2 H, d, *J* 18.3), 6.46 (3 H, dd, *J* 54.5, 7.3), 3.65 – 2.81 (8 H, m), 1.68 (1 H, s), 1.26 (6 H, t, *J* 19.3); ^{13}C NMR (125 MHz, $CDCl_3$): δ_C (126 MHz, $CDCl_3$) 170.56, 167.89, 159.27, 155.09, 153.19, 152.66, 151.57, 149.35, 133.59, 132.22, 129.66, 128.96, 128.02 (d, *J* 17.3), 126.83, 125.72, 123.87, 123.49, 122.10, 121.51, 114.51, 111.20, 109.10, 104.91, 103.35, 97.95, 77.33, 77.07, 76.82, 67.12, 65.41, 44.46, 41.45, 39.59, 12.54; HRMS (ESI, *m/z*): Calcd. for $[C_{35}H_{29}F_3N_4O_4S\text{-}H]^-$, 659.20; Found, 659.199.

2.4. Fluorescence assay of Fe^{2+} ion

The metal salts used in this study included NaCl, $CaCl_2$, $AlCl_3{\cdot}6H_2O$, $CuCl_2{\cdot}2H_2O$, $AgClO_4{\cdot}6H_2O$, $ZnCl_2$, $FeCl_3{\cdot}6H_2O$, $CoCl_2$, KCl, $HgCl_2$, $FeCl_2{\cdot}4H_2O$, $MgCl_2$, $BaCl_2$, $MnCl_2$, $CrCl_3$, $CdCl_2{\cdot}H_2O$ and $PbCl_2$. These metal salts were dissolved in ultrapure water to make a stock solution having a concentration of 100 μM for analysis. **Rh-F** was dissolved in THF to prepare a stock solution, which was then diluted with THF/H_2O to prepare an analytical solution (THF/H_2O, v/v, 7/3). The 100 μM metal ion solution and 10 μM **Rh-F** analysis solution could be directly used for absorption and fluorescence spectroscopy. In addition, different metal ion solutions and different

concentrations of Fe^{2+} analytical solutions were added dropwise to the **Rh-F** analysis solution for selectivity and sensitivity experiments, respectively. Meanwhile, fluorescence absorption was detected, and the fluorescence spectra were recorded.

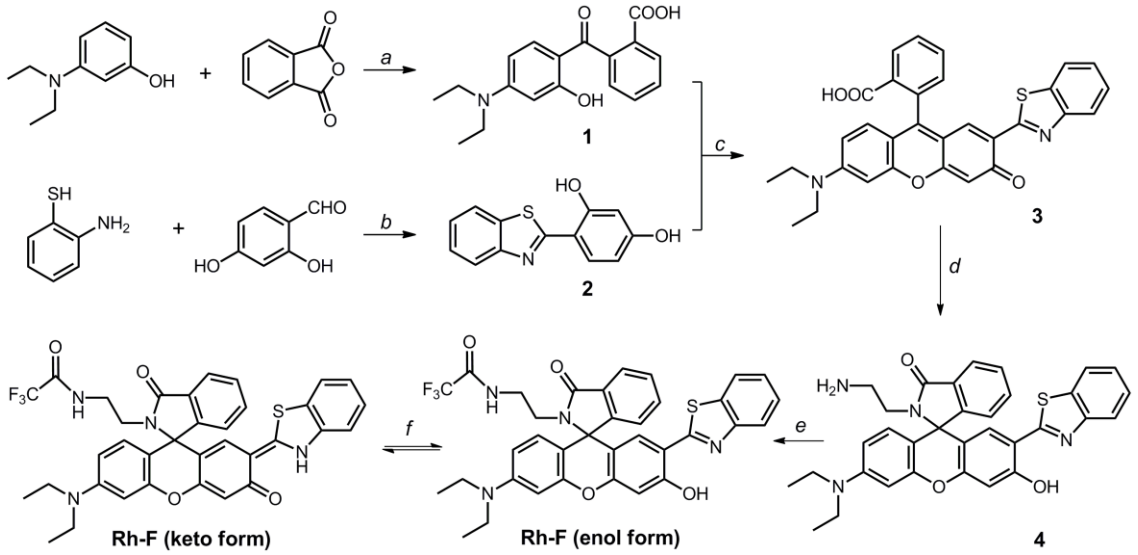

Scheme 1. (a-e) The synthetic route of **Rh-F**; (f) Equilibrium between the enol and keto forms of **Rh-F** under the ESIPT cycle.

2.5. Single crystal X-ray diffraction

Two single crystals were obtained through slow diffusion of their respective organic solutions for several days at room temperature. Because all the title crystals are stable under ambient conditions, the data collection was performed without any inert gas protection at room temperature on a Bruker SMART APEX-II CCD area detector using graphite-monochromated Mo Kα radiation (λ = 0.71073 Å). The data reduction and integration and global unit cell refinements were performed using the INTEGRATE program of the APEX2 software package. Semiempirical absorption corrections were applied using the SCALE program for the area detector. The structures were solved by direct methods and refined using the full-matrix least squares methods on F2 using SHELX

3. Results and discussion

3.1. Synthesis

The synthesis of the luminophor **Rh-F** is shown in Scheme **1**. The intermediates **1** and **2** were synthesized according to literature procedures using 3-hydroxy-*N*,*N*-diethylaniline and 2,4-dihydroxybenzaldehyde as raw materials, respectively [34-36]. Intermediate **3** was synthesized from intermediates **1** and **2** using methanesulfonic acid as solvent at 90 °C to give a dark purple solid in 56.7% yield. Intermediate **3** and ethylenediamine were refluxed in ethanol solution and purified by column chromatography to give a yellowish solid compound **4** which was excited by ultraviolet light to produce yellowish green fluorescence with a yield of 42%. Finally, compound **4** was dissolved in 1,4-dioxane solution and reacted with sodium borohydride and trifluoroacetic acid to obtain the target product as a white powder **Rh-F** (enol form) in a yield of 78.2%. The details of the synthesis and purification processes of the relevant compounds as well as the ^{1}H and ^{13}C NMR data and the mass spectrometry data results are both given in the Supplementary Materials.

3.2. The ESIPT and AIE characteristics

The new benzothiazole-modified rhodol luminophor **Rh-F** is based on the AIE+ESIPT structure. The ESIPT process of **Rh-F** was explored first. An excellent ESIPT between the phenolic hydroxyl protons and the aromatic nitrogen in the benzothiazole unit takes place upon photoexcitation which can convert the enol form to a ketone form in a short time through intramolecular hydrogen bonding (Scheme 1f). The excited keto tautomer relaxes to the ground state with fluorescence emission and then returns to its intensively favored ground state enol tautomers through ground state intramolecular proton transfer (GSIPT).

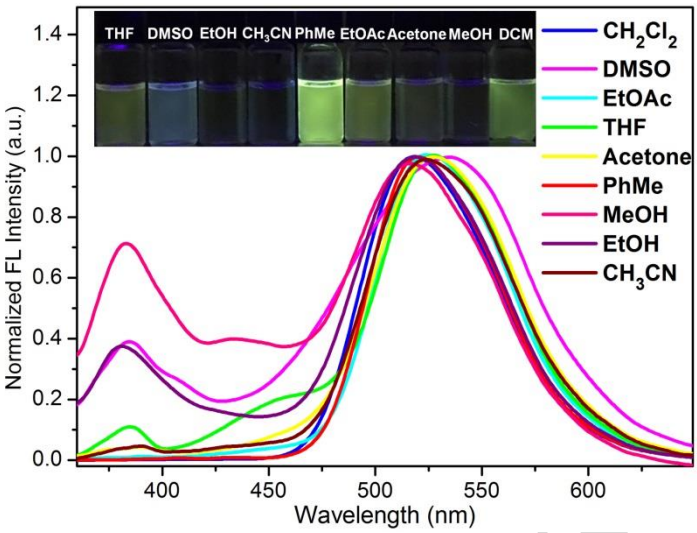

Figure 1. Normalized FL spectra of **Rh-F** in different solvents (λ_{ex} = 350 nm); Inset: Images of **Rh-F** in different solvents under a 365 nm UV lamp.

The dual emission of the enol-form type (high energy, low Stokes shift) and the keto-form type (low energy, high Stokes shift) is a typical characteristic of ESIPT fluorophores. To verify the ESIPT mechanism of **Rh-F**, we studied the emission behaviors of **Rh-F** in different solvents (Figure 1). Under excitation at 350 nm in the highly polar solvents {ethanol, methanol, tetrahydrofuran (THF) and dimethyl sulfoxide (DMSO)}, the double emission of enol and keto tautomers of **Rh-F** (about 384 and 520 nm) with low fluorescence quantum yields (Φ_F) were observed, respectively. On the basis of our previous research results, the emission at approximately 384 nm originates from the enol form. The presence of hydrogen bonds between these highly polar solvents and the phenolic hydroxyl groups of **Rh-F** can stabilize the enol form to obstruct the occurrence of the ESIPT process. The emission band at approximately 520 nm originates from the keto form induced by the ESIPT process. In non-polar or low-polar solvents {toluene, dichloromethane (DCM), ethyl acetate, acetonitrile, and acetone}, only the keto-form emission occurred at about 520 nm, which showed a large Stokes shift and relatively high fluorescence quantum yields.

In addition, we also analyzed the single crystal structure of **Rh-F** (Figure 2 and Table S1). It can

be seen that there is a strong intramolecular OH···N hydrogen bond in the structure of **Rh-F** with the corresponding distance of 1.92 Å. Furthermore, the dihedral angle between xanthene plane and benzothiazole ring plane is only 7.26 º, almost in the same plane. The pre-existing intramolecular hydrogen bond and coplane of rhodol with benzothiazole will facilitate intramolecular proton transfer and generate the photoinduced structural transformation of rhodol from the phenol (or enol) form to the keto form. Moreover, from the crystal packing of **Rh-F**, we observed that the hyper-conjugated planar construction of rhodol-benzothiazole results in the formation of intermolecular π–π stacking of **Rh-F** with the interaction distance of 3.41 Å (Figure 2b). This will limit the rotation of the C–C single bond between rhodol and benzothiazole to promote the ESIPT process.

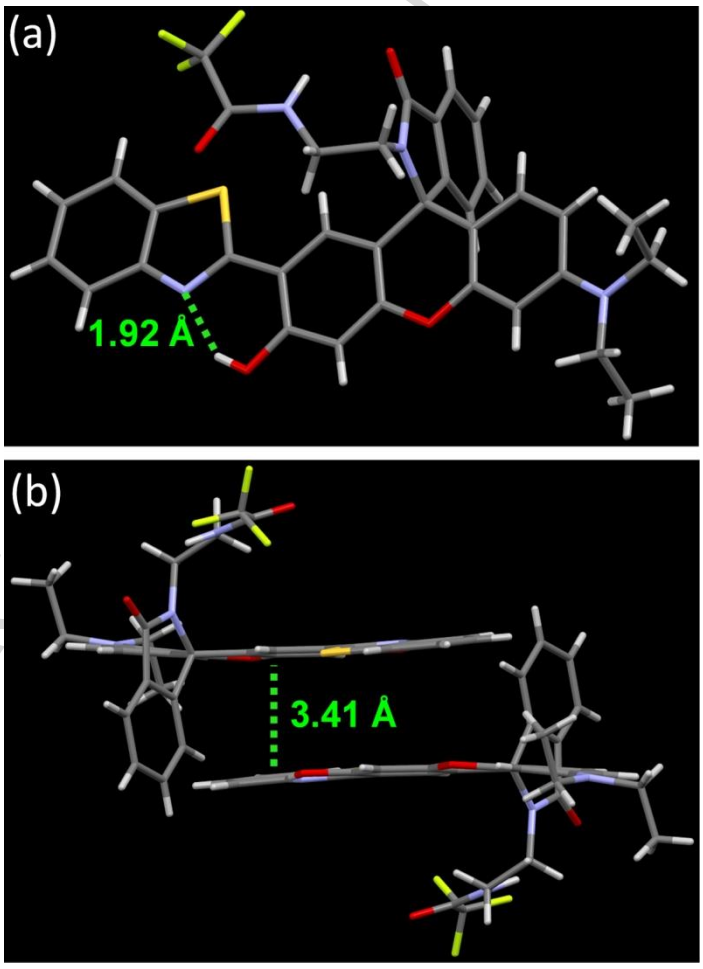

Figure 2. (a) X-ray single crystal structures of **Rh-F** showing the intramolecular OH···N hydrogen bonds; (b) The crystal packing of **Rh-F** showing the intermolecular hydrogen bonding and the π–π stacking.

Rh-F also exhibited AIE characteristics, and we have finished the following investigation. **Rh-F** showed very faint fluorescence in pure THF solution with Φ_F = 0.07, while **Rh-F** solid powder showed strong fluorescence with Φ_F = 0.56 (Figure S1). The above phenomenon indicates that **Rh-F** has AIE characteristics. To further prove this view, we studied the fluorescence properties of **Rh-F** in THF/water mixtures with different water fractions (f_w) (Figure 3a), and **Rh-F** exhibited a very interesting fluorescent spectral change. As the water fractions (f_w) gradually increased from 0% to 70%, we observed that the keto emission at 524 nm (ESIPT) decreased gradually until almost fully quenched, and simultaneously the enol emission at 384 nm was slightly enhanced. However, when the water volume fraction reached 80%, the fluorescence intensity of the keto emission at 522 nm exhibited a remarkable increase (Figure 3a inset). This can also be demonstrated by the fluorescent image under UV illumination (Figure 3c). The UV–vis absorption spectra of **Rh-F** in THF/water mixtures showed outstanding changes at $f_w \geq$ 80%, which were consistent with the emission spectra. It is not difficult to explain this phenomenon. In the THF/H_2O solution with relatively low water content ($f_w \leqq$ 70%), the intermolecular hydrogen bonds between the phenolic hydroxyl groups of rhodol and H_2O molecules are easier to form. An increase in the water content can stabilize the enol form of **Rh-F** to restrain the ESIPT process upon being excited, resulting in the keto-form emission (524 nm) decreasing and enol-form emission (384 nm) increasing. When the water content exceeds this threshold concentration (≧80%), the solubility of **Rh-F** sharply decreased and **Rh-F** separated from the solution rapidly and aggregated, thereby increasing the emission intensity of keto form due to the ESIPT.

To gain more insight into the mechanism, PL decay measurements of the solid and the methanol solution of **Rh-F** were employed, as shown in Figure 3b. Comparing the decay profiles of the solid

powder and the methanol solution samples, the fluorescence lifetime of **Rh-F** in the solid powder (5.90 ns) is longer than it is in methanol solution (1.03 ns), and that results from the facilitated radiative decay in the aggregates emission. Furthermore, the PL decay curve of the methanol solution of **Rh-F** can be fitted to a second-order exponential decay. The decay times of the fast and slow components are respectively 0.92 and 6.56 ns. Evidently, the shorter lifetime (0.92 ns) should be attributed to the enol form of **Rh-F**. The longer lifetime (6.56 ns) originates from the keto emission of **Rh-F** (ESIPT), which conforms to the lifetime of the solid powder of **Rh-F** (5.90 ns). The results are consistent with the dual emission of the methanol solution of **Rh-F** with both enol and keto emission, as shown in Figure 1.

From the above results, we can conclude that the molecular aggregation of **Rh-F** through π–π stacking can facilitate the ESIPT process, while the ESIPT process can also promote the AIE effect, resulting in the enhanced fluorescent emission in the aggregated state. Based on the coupling of ESIPT-AIE mechanisms, **Rh-F** could exhibit no self-extinguishing at high concentrations and strong emission in the aggregated state with a large Stokes shift.

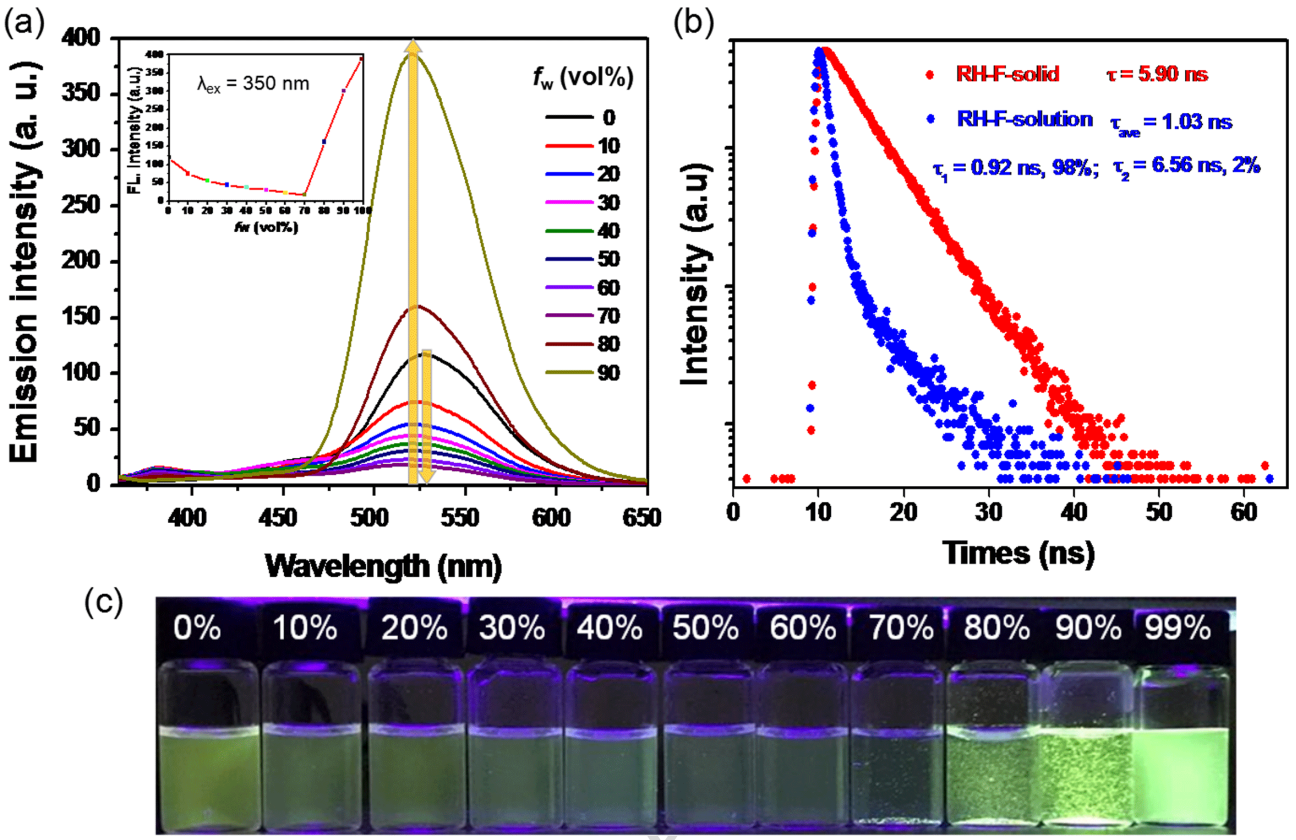

Figure 3. (a) Emission spectra of **Rh-F** (10 μM) in THF/water mixtures with different water fractions (0 - 90%), Inset: plots of the maximum emission intensity of **Rh-F** in THF/water mixtures with different water fractions (0 - 99%); (b) Fluorescence decay profiles of the **Rh-F** solid and the methanol solution of **Rh-F**; (c) Images of **Rh-F** in THF/water mixtures with different water fractions (0 - 99%) under a 365 nm UV lamp.

3.3. Sensing for Fe^{2+}

To gain insight into the fluorescence properties of the **Rh-F** probe towards metal ions, a sensing experiment of **Rh-F** was carried out in a THF/H_2O (7:3, v/v, pH = 7.4) solution. Various metal ion solutions (100 μM) were added separately to the 10 μM **Rh-F** analysis solution. The fluorescent spectra were recorded, and the results are shown in Figure 4a. The **Rh-F** solution (10 μM) showed a high fluorescence intensity on excitation at 350 nm. There is almost no apparent change in fluorescence intensity with adding Na^+, K^+, Pb^{2+}, Mg^{2+}, Ca^{2+}, Cu^{2+}, Zn^{2+}, Co^{2+}, Ag^+, Cd^{2+}, Hg^{2+}, Mn^{2+}, Fe^{3+}, Cr^{3+}, and Al^{3+} ion. However, only when Fe^{2+} was added to the **Rh-F** solution, the fluorescence intensity at 384 nm and 525 nm showed a remarkable quenching (Figure 4a). At the

same time, we can observe with naked eyes that the color of the fluorescent sensor **Rh-F** solution changes from colorless (blank and with other metal ions) to yellow (after adding Fe^{2+}) (Figure 5, top). The corresponding Figure 5 (bottom) shows the fluorescence change under UV light in 10 μM **Rh-F** solution with different metal ions. When adding Fe^{2+}, the fluorescence of the **Rh-F** solution is quenched. This indicates that Fe^{2+} complexed with **Rh-F** with its own specific paramagnetic nature to participate in the electron/energy transfer leads to the closure of the ESIPT, the inactivation of the radioactive channel of the fluorophore, and the loss of fluorescence. The occurrence of these phenomenon confirmed that **Rh-F** has the capacity for "naked-eye" discrimination of Fe^{2+} in aqueous solution.

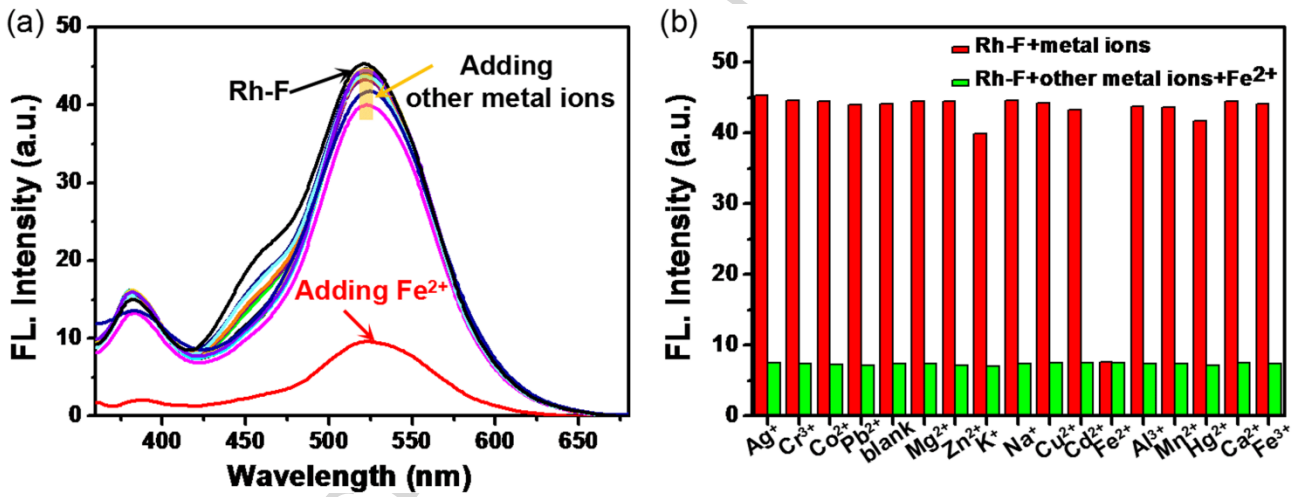

Figure 4. (a) Fluorescence emission spectra of **Rh-F** probe (10 μM) treated with 10 equiv. of various metal ions in a mixed solution of THF/H_2O (7:3, v/v, pH = 7.4); (b) Fluorescence responses of probe **Rh-F** (10 μM) to various metal ions (100 μM) at 525 nm in the absence and presence of Fe^{2+} in a mixed solution of THF/H_2O (7:3, v/v, pH = 7.4). Red bar: probe **Rh-F** with various metal ions. Green bar: probe **Rh-F** with various metal ions in the presence of Fe^{2+}.

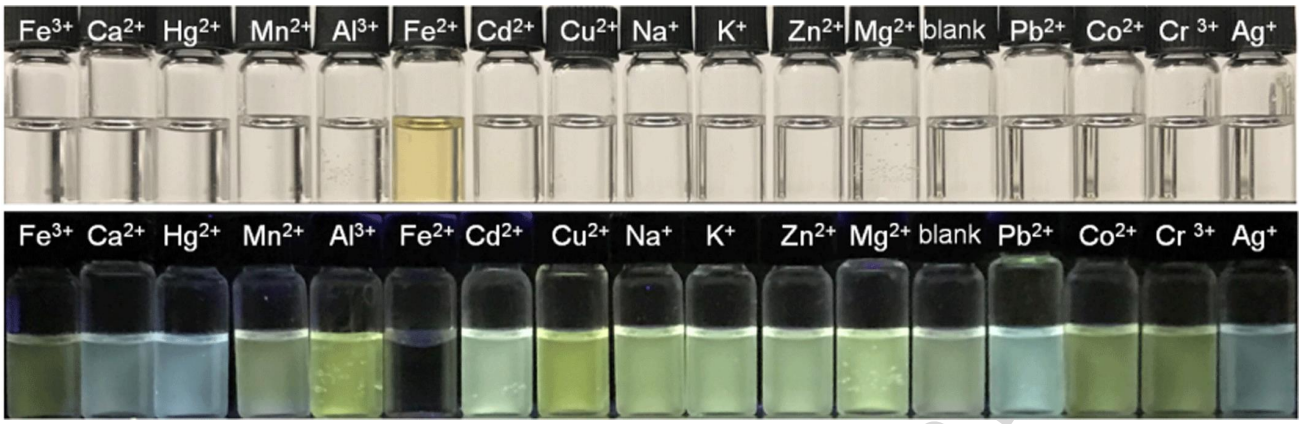

Figure 5. Color changes of **Rh-F** probe (10 μM) solutions after the addition of various metal ions (10 equiv.) under natural light (Top) and a 365 nm UV lamp (Bottom).

To further estimate the specificity of **Rh-F**, competitive experiments in the presence of Fe^{2+} mixed with other competitive metal ions were carried out. Competitive ions were initially added into the detection solution, then Fe^{2+} ion was added. The changes in fluorescence intensity at 525 nm before and after the addition of Fe^{2+} are displayed in Figure 4b. The results demonstrated that the emission of **Rh-F** at 525 nm was effectively quenched by Fe^{2+} ions with or without these metal ions. This observation confirms that the competing ions do not interfere with the sensitivity of the probe for Fe^{2+}.

To further elicit the interactions between probe **Rh-F** and Fe^{2+}, the sensitivity of **Rh-F** for Fe^{2+} was also investigated using UV-visible absorption (Figure S2) and fluorescence titration experiments (Figure 6). As shown in Figure 6a, upon treatment with increasing concentrations of Fe^{2+}, the fluorescence intensity of **Rh-F** continuously decreases and no change of the maximum emission wavelength was observed. The result indicates that when Fe^{2+} is combined with **Rh-F**, the fluorophore and the receptor cannot be integrated under the excited state, resulting in no significant change of the maximum emission wavelength. A good linear relationship between the fluorescence intensity and Fe^{2+} concentration in range of 0-1.0 μM was determined (Figure 6b, R^2 = 0.99099). In

addition, the detection limit of the **Rh-F** probe for Fe^{2+} is about 115.2 nM, which is sufficiently low for the detection of Fe^{2+} ions found in many environmental and biological systems.

To optimize the experimental conditions for the detection of Fe^{2+}, the response time between **Rh-F** and Fe^{2+} and the fluorescence intensity of probe **Rh-F** and **Rh-F** + Fe^{2+} complexes in different pH were investigated. The result showed that the fluorescence intensity of **Rh-F** + Fe^{2+} (2 equiv) reduced to a minimum value within 4 minutes (Figure S3a), indicating that the probe **Rh-F** could detect Fe^{2+} rapidly. In addition, as shown in Figure S3b, no significant changes in the fluorescence intensity at 525 nm was observed for both the free probe **Rh-F** and **Rh-F** + Fe^{2+} complex in the range of pH 2-13. It indicated that the probe **Rh-F** and **Rh-F** + Fe^{2+} had good stability upon acidic and alkaline conditions. Compared the fluorescence intensity of **Rh-F** and **Rh-F** + Fe^{2+}, it showed that when the probe **Rh-F** treated with 2 equiv of Fe^{2+}, the fluorescence of the probe **Rh-F** is quenched in the range of pH 2-13. The reslut indicated that the probe **Rh-F** is suitable for the detection of Fe^{2+} in any pH condition.

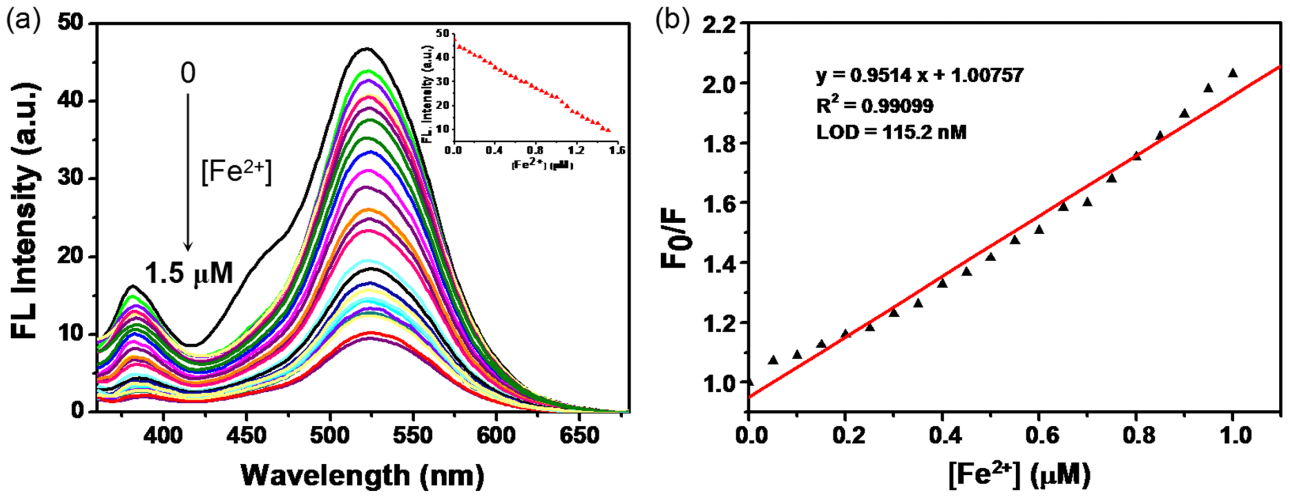

Figure 6. (a) Fluorescence response of the **Rh-F** (10 μM) probe upon incubation with increasing concentrations of Fe^{2+} (0 - 1.5 μM). Inset: plot of the emission intensity at 525 nm as a function of the concentrations of Fe^{2+}. (b) Linear plots of fluorescence intensity as a function of Fe^{2+} concentrations (0 - 1.0 μM).

3.4. The proposed sensing mechanism

Further studies were carried out to explore the mechanism of sensing Fe^{2+}. We proposed the possible mechanism which is shown in Figure 7a. The ^{1}HNMR titration of the free **Rh-F** shows the characteristic phenolic hydroxyl proton signal at 12.836 ppm (Figure S4a), and the phenolic hydroxyl proton signal disappeared when the 1.0 μM Fe^{2+} was added (Figure S4b). The mechanism of fluorescence quenching when **Rh-F** combined with Fe^{2+} may be caused by the following two factors. First, with the addition of Fe^{2+} to the **Rh-F** solution, Fe^{2+} chelated with the O atom of the hydroxyl group and the N atom of the benzothiazole moiety (Figure 7a). This might cause the ESIPT process of the **Rh-F** to be devastated and the keto-type emission decreased. The second reason may result from the paramagnetic properties of Fe^{2+}. Figure 7b showed the curve fitting of **Rh-F** receptor fluorescence intensity against the reciprocal of the Fe^{2+} concentration with the Benesi-Hildebrand equation based on fluorescence titration. The binding constant K_a of **Rh-F** with Fe^{2+} had been established (K_a= 1.31 × 10^5, R^2 = 0.98171). The linear curve fit provides evidence for the 1:1 complexation behavior of **Rh-F** to Fe^{2+}. Simultaneously, we also carried out a Job's plot (Figure 7c) and the lowest intensity change point appeared at about 0.5, this provides further confirmation that **Rh-F** formed a 1:1 stoichiometry complex with Fe^{2+}. Furthermore, the binding mode of **Rh-F** and Fe^{2+} was confirmed by the FT-IR (Figure S5) and HRMS (Figure S8). Comparing the FT-IR of **Rh-F** with **Rh-F**-Fe^{2+}, upon the addition of 1.0 equiv Fe^{2+}, the absorption peak of the phenolic hydroxyl group at 3218.14 cm^{-1} disappeared. The absorption peak of C=N valence vibration underwent a redshift from 1473 to 1492 cm^{-1}. These results indicated that the complexation between **Rh-F** and the iron center resulted in the occurrence of a strong weakening of the C=N bond. In the HRMS of **Rh-F**-Fe^{2+}, the characteristic peak of [**Rh-F** + H]$^+$ at m/z 659.19 completely disappeared (Figure S7) and

a new peak arose at m/z 749.19 which was assigned to [**Rh-F**-Fe^{2+} + H]$^{+}$. The above results confirmed the binding mechanism proposed in Figure 7a. The destruction of the ESIPT process of **Rh-F** was caused by the chelation of Fe^{2+} with the O atom of the hydroxyl group and the N atom of the benzothiazole moiety, which resulted in the quenching of the **Rh-F** fluorescence sensor.

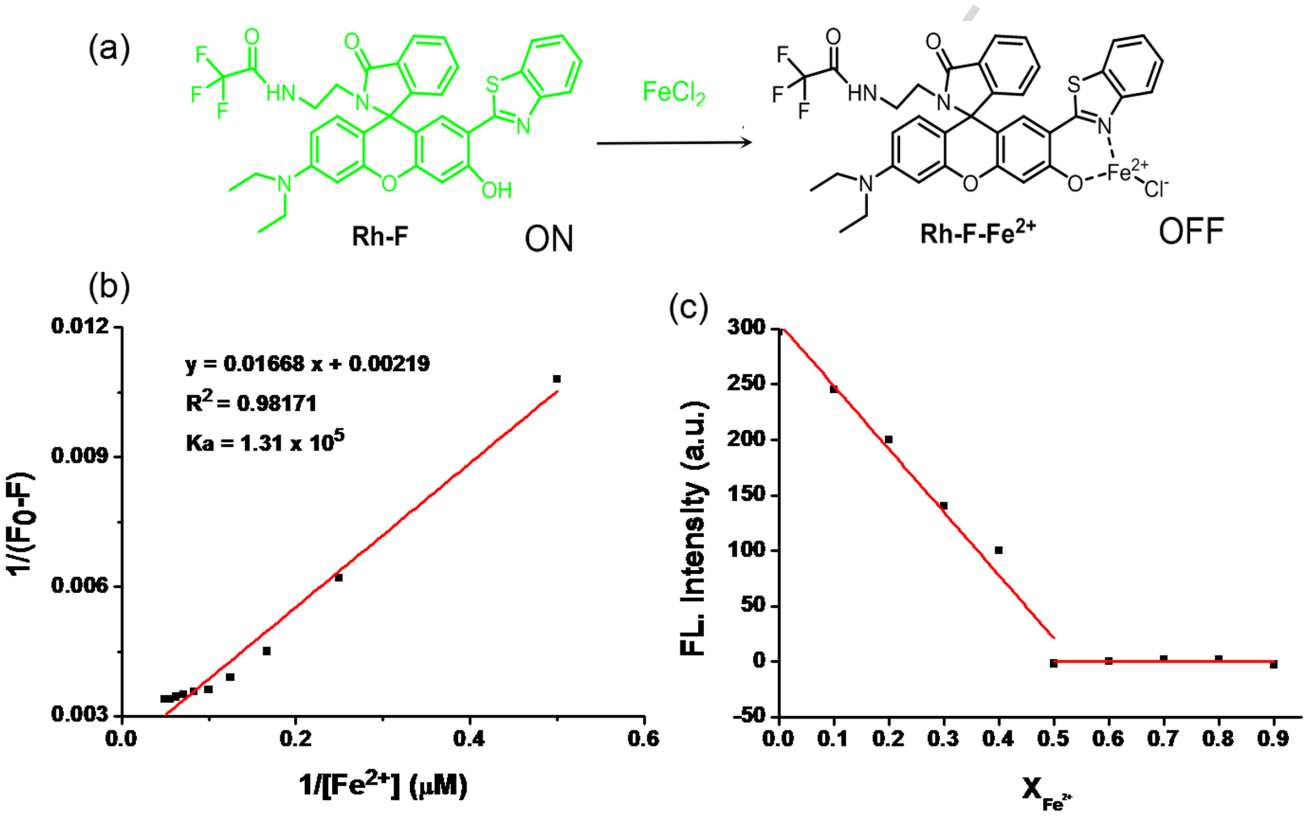

Figure 7. (a) Sensing mechanism of the **Rh-F** probe for Fe^{2+}; (b) Benesi-Hildebrand plot for the determination of the binding constant of **Rh-F** (10 μM) for Fe^{2+} in a mixed solution of THF/H_2O (7:3, v/v, pH = 7.4) (λ_{ex} = 350 nm); (c) Job's plot for determining the stoichiometry of **Rh-F** with Fe^{2+} in a mixed solution of THF/H_2O (8:2, v/v, pH = 7.4) (λ_{ex} = 350 nm), $X_{Fe^{2+}}$ = [Fe^{2+}]/{[Fe^{2+}] + [**Rh-F**]}.

4. Conclusions

In conclusion, we introduced the benzothiazole into the xanthene ring of Rhodol to design and synthesize a new **Rh-F** fluorophore based on the dual mechanism of AIE-ESIPT. Due to the mutual synergy between ESIPT and AIE mechanisms, it exhibited excellent photophysical properties such as solvent dependent emission behavior, efficient aggregated emission around 525 nm, and a large

Stokes shift (>180 nm). Furthermore, the **Rh-F** fluorophore exhibited outstanding identification ability for Fe^{2+}. It is a sensor with high selectivity and sensitivity, which mainly utilized the ESIPT mechanism and the polymerization fluorescence method of **Rh-F**. This work can stimulate us to easily develop fluorescent sensors for different analytes with the AIE/ESIPT mechanism by modifying the phenolic hydroxyl functional groups in the Rhodol ring. The development of AIE/ESIPT fluorophores will provide a viable design strategy for biosensors.

Acknowledgments

We gratefully acknowledge the National Natural Science Foundation of China (21202132, 21505105, and 21874108), China Postdoctoral Science Foundation (2016M592837), and the Open Foundation of State Key Laboratory of Crystal Materials (KF1806) for funding.

References

[1] A. Ekbote, S.H. Han, T. Jadhav, S.M. Mobin, J.Y. Lee, R. Misra, Stimuli responsive AIE active positional isomers of phenanthroimidazole as non-doped emitters in OLEDs, J. Mater. Chem. C 6 (2018) 2077−2087.

[2] N. Venkatramaiah, G.D. Kumar, Y. Chandrasekaran, R. Ganduri, S. Patil, Efficient blue and yellow organic light-emitting diodes enabled by aggregation-induced emission, ACS Appl. Mater. Interfaces 10 (2018) 3838−3847.

[3] Y. Wang, Y Liao, C.P. Cabry, D. Zhou, G. Xie, Z. Qu, D.W. Bruce, W. Zhu, Highly efficient blueish-green fluorescent OLEDs based on AIE liquid crystal molecules: from ingenious molecular design to multifunction materials, J. Mater. Chem. C 5 (2017) 3999−4008.

[4] S. Biswas, R. Mengji, S. Barman, V. Venugopal, A. Jana, N.D.P. Singh, 'AIE + ESIPT' assisted photorelease: fluorescent organic nanoparticles for dual anticancer drug delivery with real-time monitoring ability, Chem. Commun. 54 (2018) 168−171.

[5] C. B. Bai, H.Y. Fan, R. Qiao, S.N. Wang, B. Wei, Q. Meng, Z.Q. Wang, J.X. Liao, J. Zhang, L. Zhang, S.S. Chen, H. Miao, Synthesis of methionine methyl ester-modified coumarin as the fluorescent-colorimetric chemosensor for selective detection Cu^{2+} with application in molecular logic gate, Spectrochim. Acta Part A 216 (2019) 45−51.

[6] S. Chen, W.J. Wang, M.M. Yan, Q. Tu, S.W. Chen, T.B. Li, M.S. Yuan, J.Y. Wang, 2-Hydroxy benzothiazole modified rhodol: aggregation-induced emission and dual-channel fluorescence sensing of Hg^{2+} and Ag^{+} ions, Sens. Actuators B 255 (2018) 2086−2094.

[7] D. Dahal, K.R. Ojhaa, N. Alexander, M. Konopkaa, Y. Pang, An NIR-emitting ESIPT dye with large stokes shift for plasma membrane of prokaryotic (*E. coli*) cells, Sens. Actuators B 259 (2018) 44−49.

[8] P. Gopikrishna, N. Meher, P.K. Iyer, Functional 1,8-naphthalimide AIE/AIEEgens: recent advances and prospects, ACS Appl. Mater. Interfaces 10 (2018) 12081−12111.

[9] V.S. Padalkar, S. Sek, Excited-state intramolecular proton-transfer (ESIPT)-inspired solid state emitters, Chem. Soc. Rev. 45 (2016) 169−202.

[10] L. Chen, D .Wu, C.S. Lim, D. Kim, S.J. Nam, W. Lee, G. Kim, H.M. Kim, J. Yoon, A two-photon fluorescent probe for specific detection of hydrogen sulfide based on a familiar ESIPT fluorophore bearing AIE characteristics, Chem. Commun. 53 (2017) 4791−4794.

[11] S. Janakipriy, S. Tamilmani, S. Thennarasu, A novel 2-(2′-aminophenyl)benzothiazole derivative displays ESIPT and permits selective detection of Zn^{2+} ions: experimental and theoretical studies, RSC Adv. 6 (2016) 71496−71500.

[12] L. Chen, S.Y. Yin, M. Pan, K. Wu, H.P. Wang, Y.N. Fan, C.Y. Su, A naked eye colorimetric sensor for alcohol vapor discrimination and amplified spontaneous emission (ASE) from a highly fluorescent excited-state intramolecular proton transfer (ESIPT) molecule, J. Mater. Chem. C. 4 (2016) 6962−6966.

[13] L. Yan, T. Qing, R. Li, Z. Wang, Z. Qi, Synthesis and optical properties of aggregation-induced emission (AIE) molecules based on the ESIPT mechanism as pH- and Zn^{2+}-responsive fluorescent sensors, RSC Adv. 6 (2016) 63874−63879.

[14] Y. Liu, J. Nie, J. Niu, W. Wang, W. Lin, An AIE + ESIPT ratiometric fluorescent probe for monitoring sulfur dioxide with distinct ratiometric fluorescence signals in mammalian cells, mouse embryonic fibroblast and zebrafish, J. Mater. Chem. B 6 (2018) 1973−1983.

[15] Y. Chen, T. Wei, Z. Zhang, T. Chen, J. Li, J. Qiang, J. Lv, F. Wang, X. Chen, A benzothiazole-based fluorescent probe for ratiometric detection of Al^{3+} in aqueous medium and living cells, Ind. Eng. Chem. Res. 56 (2017) 12267−12275.

[16] Q. Chen, C. Jia, Y. Zhang, W. Du, Y. Wang, Y. Huang, Q. Yang, Q. Zhang, A novel fluorophore based on the coupling of AIE and ESIPT mechanisms and its application in biothiol imaging, J. Mater. Chem. B 5 (2017) 7736−7742.

[17] F. Liu, P. Tang, R. Ding, L. Liao, L. Wang, M. Wang, J. Wang, A glycosylation strategy to develop a low toxic naphthalimide fluorescent probe for the detection of Fe^{3+} in aqueous medium, Dalton Trans. 46 (2017) 7515–7522.

[18] N.R. Chereddy, K. Suman, P.S. Korrapati, S. Thennarasu, A.B. Mandal, Design and synthesis of rhodamine based chemosensors for the detection of Fe^{3+} ions, Dyes Pigment 95 (2012) 606−613.

[19] J. Zhang, C. Cai, S. Razzaque, I. Hussain, Q.W. Lu, B. Tan, Synthesis of water-soluble and highly fluorescent gold nanoclusters for Fe^{3+} sensing in living cells using fluorescence imaging, J.

Mater. Chem. B 5 (2017) 5608−5615.

[20] Z. Zhang, F. Li, C. He, H. Ma, Y. Feng, Y. Zhang, M. Zhang, Novel Fe^{3+} fluorescence probe based on the charge-transfer (CT) molecules, Sens. Actuators B 255 (2018) 1878–1883.

[21] Y. Gao, H. Liu, Q. Liu, W. Wang, A novel colorimetric and OFF–ON fluorescent chemosensor based on fluorescein derivative for the detection of Fe^{3+} in aqueous solution and living cells, Tetrahedron Lett. 57 (2016) 1852−1855.

[22] S.D. Padghan, A.L. Puyad, R.S. Bhosale, S.V. Bhosale, S.V. Bhosale, A pyrene based fluorescent turn-on chemosensor: aggregation-induced emission enhancement and application towards Fe^{3+} and Fe^{2+}recognition, Photochem. Photobiol. Sci. 16 (2017) 1591–1595.

[23] B. Zhao, T. Liu, Y. Fang, L. Wang, B. Song, Q. Deng, Two 'turn-off' schiff base fluorescence sensors based on phenanthro[9,10-d]imidazole-coumarin derivatives for Fe^{3+} in aqueous solution, Tetrahedron Lett. 57 (2016) 4417–4423.

[24] Z. Guo, Q. Niu, T. Li, Highly sensitive oligothiophene-phenylamine-based dual-functional fluorescence "turn-on" sensor for rapid and simultaneous detection of Al^{3+} and Fe^{3+} in environment and food samples, Spectrochim. Acta Part A 200 (2018) 76–84.

[25] K.P. Wang, Y. Lei, S.J. Zhang, W.J. Zheng, J.P. Chen, S. Chen, Q. Zhang, Y.B. Zhang, Z.Q. Hu, Fluorescent probe for Fe(III) with high selectivity and its application in living cells, Sens. Actuators B 252 (2017) 1140−1145.

[26] B. Bag, B. Biswal, Alteration of selectivity in rhodamine based probes for Fe(III) and Hg(II) ion induced dual mode signalling responses, Org. Biomol. Chem. 10 (2012) 2733−2738.

[27] L. Wang, Y.Q. Fan, X.W. Guan, W.J. Qu, Q. Lin, H. Yao, T.B. Wei, Y.M. Zhang, A novel naphthalimide–glutathione chemosensor for fluorescent detection of Fe^{3+} and Hg^{2+} in aqueous medium and its application, Tetrahedron 74 (2018) 4005−4012.

[28] B. Shen, Y. Qian, Building rhodamine-BODIPY fluorescent platform using click reaction: naked-eye visible and multi-channel chemodosimeter for detection of Fe^{3+} and Hg^{2+}, Sens. Actuators

B 260 (2018) 666–675.

[29] L. Jin, C. Liu, N. An, Q. Zhang, J. Wang, L. Zhao, Y. Lu, Fluorescence turn-on detection of Fe^{3+} in pure water based on a cationic poly(perylene diimide) derivative, RSC Adv. 6 (2016) 58394–58400.

[30] K. Kawai, N. Ieda, K. Aizawa, T. Suzuki, N. Miyata, H. Nakagawa, A reductant-resistant and metal-free fluorescent probe for nitroxyl applicable to living cells, J. Am. Chem. Soc. 135 (2013) 12690−12696.

[31] M. Taki, K. Akaoka, K. Mitsui, Y. Yamamoto, A mitochondria-targeted turn-on fluorescent probe based on a rhodol platform for the detection of copper(I), Org. Biomol. Chem. 12 (2014) 4999–5005.

[32] Y. Zhang, L. Ma, C. Tang, S. Pan, D. Shi, S. Wang, M. Li, Y. Guo, A highly sensitive and rapidly responding fluorescent probe based on a rhodol fluorophore for imaging endogenous hypochlorite in living mice, J. Mater. Chem. B 6 (2018) 725−731.

[33] E.A. Halabi , Z. Thiel , N. Trapp, D. Pinotsi, P.R. Fuentes, A photoactivatable probe for super-resolution imaging of enzymatic activity in live cells, J. Am. Chem. Soc. 139 (2017) 13200−13207.

[34] H. Wang, J.P. Guan, X. Han, S.W. Chen, T.B. Li, Y.R. Zhang, M.S. Yuan, J.Y. Wang, Benzothiazole modified rhodol as chemodosimeter for the detection of sulfur mustard simulant, Talanta 189 (2018) 39–44.

[35] H. Wen, Q. Huang, X.F. Yang, H. Li, Spirolactamized benzothiazole-substituted N,N-diethylrhodol: a new platform to construct ratiometric fluorescent probes, Chem. Commun. 49 (2013) 4956−4958.

[36] Q. Wang, L. Zhou, L. Qiu, D. Lu, Y. Wu, X.B. Zhang, An efficient ratiometric fluorescent probe for tracking dynamic changes in lysosomal pH, Analyst 140 (2015) 5563–5569.

Graphical Abstract

A new Benzothiazole-rhodol based fluorescent probe was constructed facilely with ESIPT-induced AIE and an application for Detecting Fe^{2+} Ion.

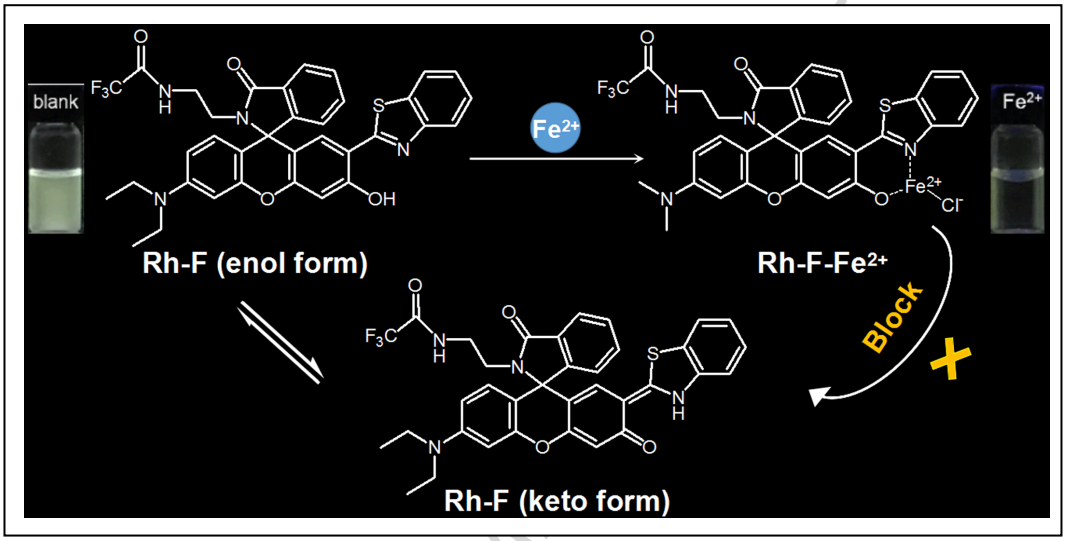

Highlights:

> Rh-F exhibited excellent synergistic effect of AIE and ESIPT feature.

> Rh-F achieves "on-off" fluorescence and visual color change for detecting Fe^{2+}.

> Rh-F showed a sensitive fluorescence response to Fe^{2+} with high selectivity.